Cargo-Binding Makes a Wild-Type Single-Headed Myosin-VI Move Processively

Mitsuhiro Iwaki,*† Hiroto Tanaka,† Atsuko Hikikoshi Iwane,‡ Eisaku Katayama,§ Mitsuo Ikebe,¶ and Toshio Yanagida*†‡

*Department of Biophysical Engineering, Osaka University, Suita, Osaka, Japan; †Formation of Soft Nanomachines, Core Research for Evolution Science and Technology, Japan Science and Technology Agency, Suita, Osaka, Japan; ‡Soft Biosystem Group, Laboratories for Nanobiology, Graduate School of Frontier Biosciences, Osaka University, Suita, Osaka, Japan; §Division of Biomolecular Imaging, Institute of Medical Science, The University of Tokyo, Minato-ku, Tokyo, Japan; and ¶University of Massachusetts Medical School, Worcester, Massachusetts

ABSTRACT Class VI myosin is an intracellular vesicle and organelle transporter that moves along actin filaments in a direction opposite to most other known myosin classes. The myosin-VI was expected to form a dimer to move processively along actin filaments with a hand-over-hand mechanism like other myosin organelle transporters. Recently, however, wild-type myosin-VI was demonstrated to be monomer and single-headed, casting a doubt on its processivity. By using single molecule techniques, we show that green-fluorescent-protein-tagged single-headed, wild-type myosin-VI does not move processively. However, when coupled to 200-nm polystyrene beads (comparable to intracellular vesicles in size) at a ratio of one head per bead, single-headed myosin-VI moves processively with large (40-nm) steps. The characteristics of this monomer-driven movement were different to that of artificial dimer-driven movement: Compared to the artificial dimer, the monomer-bead complex had a reduced stall force (1 pN compared to 2 pN), an average run length 2.5-fold shorter (91 nm compared to 220 nm) and load-dependent step size. Furthermore, we found that a monomer-bead complex moved more processively in a high viscous solution (40-fold higher than water) similar to cellular environment. Because the diffusion constant of the bead is 60-fold lower than myosin-VI heads alone in water, we propose a model in which the bead acts as a diffusional anchor for the myosin-VI, enhancing its rebinding following detachment and supporting processive movement of the bead-monomer complexes. Although a single-headed myosin-VI was able to move processively with a large cargo, the travel distance was rather short. Multiple molecules may be involved in the cargo transport for a long travel distance in cells.

INTRODUCTION

During the last decade, a number of myosin-like molecules have been discovered, making it evident that myosin constitutes a diverse superfamily (1–3). In contrast to well-known filament-forming myosins, now classified as myosin-II, newly found myosins do not form filaments and are called unconventional myosins (4). One of the most important features of these myosins is that they function as intracellular cargo carriers, thus playing a critical role in vesicular trafficking in cells. Supporting this notion, several members of the myosin superfamily have been shown to be processive motors, in which myosin travels a long distance along actin filaments without dissociation (5–9). Myosin-Va was the first of many myosins shown to be processive (5). Because myosin-Va has a double-headed structure with a long neck, it is thought that myosin-Va moves processively along an actin filament with a hand-over-hand mechanism (10–14). Subsequently, it was shown that myosin-VI, which moves along actin filaments in the opposite direction to myosin-V (15), also shows processive movement (7,8) with a hand-over-hand mechanism (16,17). The myosin-VI constructs tested were double-headed by introducing a coiled-coil element at the C-terminal end of the molecule. However, it was reported quite recently that chicken wild-type myosin-VI is single-headed, casting a doubt on its processivity (18). Yet, in vivo, myosin-VI is implicated in moving endocytic vesicles into a cell (19–21).

We observed that wild-type single-headed myosin-VI without cargo did not move processively, consistent with a previous study (18). In cells, however, myosin-VI attaches a cargo to its tail end and transports it along actin filaments. The myosin head tethered to the cargo may undergo dissociation-reassociation with actin without diffusing away from the actin because of the relatively slow Brownian motion of the cargo. Therefore, we hypothesized that the cargo binding to myosin-VI may allow the myosin-VI motor to move processively. As a fact, we found in this study that myosin-VI processively moved along actin filaments with large (~40-nm) steps upon binding to a cargo. Furthermore, we found that a cargo-associated single-headed wild-type myosin-VI processively moved in a solution with viscosity similar to that of a cellular environment.

Submitted October 20, 2005, and accepted for publication January 18, 2006.

Address reprint requests to Toshio Yanagida, Soft Biosystem Group, Laboratories for Nanobiology, Graduate School of Frontier Biosciences, Osaka University, 1-3,Yamadaoka, Suita, Osaka 565-871, Japan. Tel.: 81-6-6879-4632; Fax: 81-6-6879-4634; E-mail: yanagida@phys1.med.osaka-u.ac.jp.

0006-3495/06/05/3643/10 $2.00

doi: 10.1529/biophysj.105.075721

MATERIALS AND METHODS

Proteins

Actin was obtained from rabbit skeletal muscle and purified as described (22). Biotinylated actin was prepared by linking Biotin-$(AC_5)_2$-Osu

(Dojindo, Kumamoto, Japan) to the amino-terminus of actin as described (23). Actin filaments were obtained by mixing native actin and biotinylated actin at 10:1 in buffer (0.1 M KCl, 10 mM HEPES-KOH (pH 7.8)). To visualize under an optical microscope, actin filaments were labeled with phalloidin-tetramethylrhodamine (TMR). Preparation and expression for mouse full-length (wild-type) (M6WT) and engineered double-headed myosin-VI construct (M6DH) (fused with hexahistidine tag at the C-terminus) was as described previously (8). Purification was done by His-tag affinity chromatography.

Myosin-coated beads

Fluorescent latex beads (diameter 0.2 μm, 2% solids, Molecular Probes, Eugene, OR) were incubated with 6×His monoclonal antibody (1 mg/ml, BD Biosciences, Franklin Lakes, NJ) at the molar ratio of 1:200 for 1 h at 0°C and sedimented at 21,800 × g for 5 min. The sedimented beads were suspended in buffer (25 mM KCl, 20 mM HEPES-KOH (pH 7.8 or 7.1), 5 mM MgC_{12}, and 1 mM EGTA) and sedimented again. This process was repeated three times. The number of 6×His antibody molecules bound to a bead was estimated to be at least 50. 1 μl of 6×His antibody-coated beads was incubated for 10 min in assay buffer containing 10 mg/ml bovine serum albumin (Sigma-Aldrich, St. Louis, MO) and His-tagged M6WT or M6DH. The beads were observed within 30 min after preparation.

Single-molecule nanometry

Sample chambers with 10-μl capacity were made by placing a coverslip over a glass slide separated by two parallel slips of polyester film ~25 μm in thickness. Fluorescently labeled actin filaments containing biotinylated G-actin (10% of total G-actin) were bound to a glass surface that had been coated with avidin-biotinylated bovine serum albumin. Myosin tagged beads at 3–10 pM in assay buffer (25 mM KCl, 20 mM HEPES-KOH (pH 7.8 or 7.1), 5 mM $MgCl_2$, 1 mM EGTA, ATP, and oxygen scavenger system (0.11 mg/ml glucose oxidase, 18 μg/ml catalase, 2.3 mg/ml glucose, and 0.5% 2-mercaptoethanol)) were introduced into the sample chamber. Myosin-VI tagged beads were optically trapped and brought into contact with actin filaments. Imaging and detection of bead positions were done as described (24,25). The response time of the 0.2-μm bead was 230 μs at 0.25 pN load, which was enough to detect stepping movement of myosin-VI at low load. All experiments were performed in assay buffer at 24°C.

Bead displacements were recorded at a sampling rate of 24 kHz with a bandwidth of 10 kHz. The load exerted on the beads was calculated from the bead displacement multiplied by the trap stiffness (~8 fN/nm), which was determined from the variance of the Brownian motion of a trapped bead by the equipartition theorem of energy. Interactions were detected as a stiffness increase (0.02–0.04 pN/nm) followed by a long dwell (>50 ms) from the raw trace, and the steps were detected as a rapid (<5-ms) positional change (larger than the standard deviation of the bead fluctuation, or 5–8 nm) followed by a long dwell (50 ms) from the Chebyshev-filtered trace. The step size was estimated from the difference between the mean prestep position and poststep position. To determine the precise step size at low load, we calculated the elastic component in our single trapping geometry and estimated the correction factor depending on load (26). At no load condition could we determine the size of each step directly without correction because of the absence of attenuation with optical trapping.

Single-molecule imaging and electron microscopy

Single-molecule imaging of green-fluorescent-protein (GFP)-tagged myosin (27,28) and electron micrographs of myosin were performed as previously described (8). Single-molecule imaging of GFP-tagged myosin-VI with fluorescent bead was performed as follows. Emission wavelength of the fluorescent bead (E_x/E_m = 600/610, Molecular Probes) was chosen not to overlay the GFP emission wavelength. Because the emission of both TMR-labeled actin filaments and the fluorescent beads are highly bright compared to that of single GFP molecules, we decided to use an excitation laser of 476-nm wavelength (which is not an optimized wavelength for TMR and fluorescent beads) to decrease these emission intensities. Finally, we simultaneously observed single GFP molecules and fluorescent beads and TMR-labeled actin filaments by choosing the dichroic mirror and filter carefully.

When we observed the GFP bound bead in a high viscous solution, the Brownian motion of the GFP molecule synchronized with that of the bead could be observed. By using this observation system, we analyzed the GFP-tagged myosin-VI binding ratio to the bead. Because of both translational and rotational Brownian motion of the bead, the fluorescence intensity of the GFP molecule was unstable. Therefore, to analyze the photobleaching process, we analyzed the GFP fluorescence on the bead stuck on the glass surface.

High viscous solution experiment

Methylcellulose (Sigma-Aldrich) was dissolved at 1% (w/v) in buffer solution (25 mM KCl, 20 mM HEPES-KOH (pH 7.8), 5 mM $MgCl_2$, and 1 mM EGTA) and stocked. The stocked methylcellulose buffer was diluted to 0.5% by adding assay buffer (25 mM KCl, 20 mM HEPES-KOH (pH 7.8), 5 mM $MgCl_2$, 1 mM EGTA, ATP, oxygen scavenger system, and 1 mg/ml Casein (Nacalai Tesque, Kyoto, Japan) and used in the experiment at 24°C.

Two-dimensional diffusion of a bead (220 nm in diameter) was tracked (> 1μm) and the diffusion coefficient was calculated by plotting the mean-square displacement versus the time interval using the equation $\langle d^2(t)\rangle = 4Dt$. Here d is the displacement, t is the time, and D is the diffusion coefficient. The calculated diffusion coefficient in water ($D = 7.9 \pm 0.3 \times 10^2$ nm^2 ms^{-1}) was consistent with that obtained from the Power spectrum density of the Brownian motion of laser-trapped bead in water (see Supplementary Material). In the condition of 0.5% (w/v) methylcellulose, the diffusion coefficient of the bead was 40 times smaller than that of water.

RESULTS

Mouse wild-type myosin-VI is a monomer and a nonprocessive motor without cargo

To confirm if mouse recombinant wild-type myosin-VI used in this study is also monomeric, we observed M6WT by electron microscopy (Fig. 1*A*). A field of rotary shadowed myosin-VI shows globular molecules followed by an ~30-nm thin extension. We observed >300 molecules and confirmed that mouse M6WT is also a monomer and single-headed. To further confirm that mouse M6WT is a monomer, we observed single GFP-tagged M6WT in motility assay solution (see Materials and Methods) by total internal reflection microscopy (27,28). In all observations (187 spots), the GFP fluorescence photobleached in a single step, suggesting that M6WT is a monomer in the motility assay, too. To test for processivity of M6WT, we observed the single-molecule interaction between GFP-tagged M6WT and an actin filament. In all observations (200 spots), the GFP-tagged M6WT did not show processive movement over a 60-nm spatial resolution (Fig. 1*B*) as shown previously (18), although the GFP-tagged M6DH did show processive movement (Fig. 1 *C*). Fig. 1 *D* shows durations of GFP-tagged M6WT (*black bars*) and GFP-tagged M6DH (*gray bars*) attachment on an actin

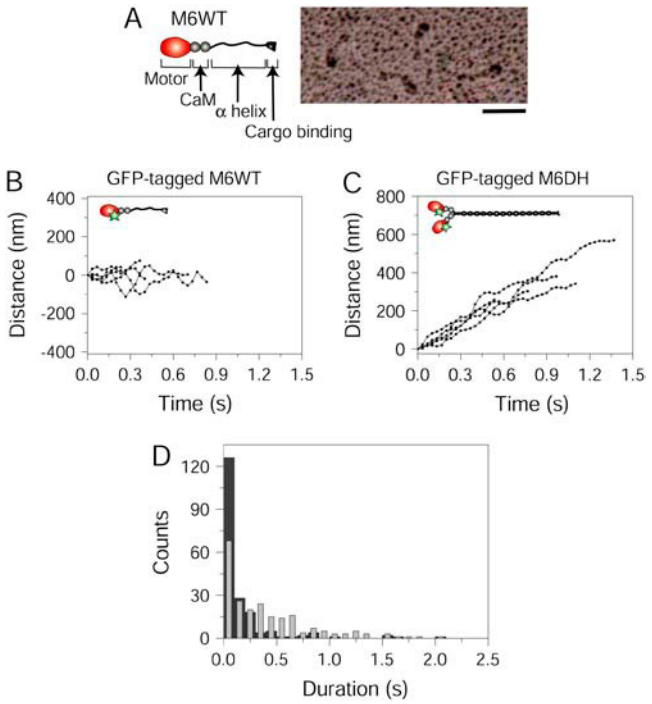

FIGURE 1 Structure and single-molecule imaging of M6WT. (*A*) Schematic drawing of M6WT. Myosin-VI consists of a motor domain (*red*), two calmodulin binding domains (*gray*), an ~30-nm-long α-helix and a cargo-binding domain (*black*). At right is an electron micrograph of rotary-shadowed M6WT. Scale bar, 50 nm. (*B* and *C*) Movement of GFP-tagged single-headed M6WT and M6DH, each without cargo. Time courses for GFP spot movements of single-headed M6WT (*B*) and M6DH (*C*) on an actin filament. (*D*) Duration of attachment of GFP-tagged single-headed M6WT (*black bars*) and GFP-tagged M6DH (*gray bars*) to an actin filament.

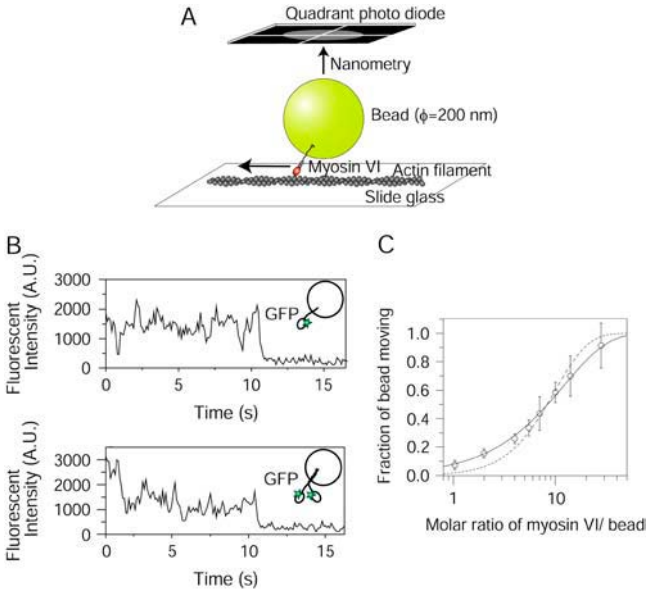

FIGURE 2 Evidence for cargo transport by a single M6WT molecule. (*A*) Measurement system. A myosin-coated bead was optically trapped and brought into contact with an actin filament attached to a glass surface. The bead image was projected onto a quadrant photodiode and the movement was determined with nanometer accuracy. (*B*) Typical photobleach of GFP on a bead stuck on the glass surface at M6WT/bead mixing stoichiometry of 2:1. (*Upper*) GFP-tagged M6WT on a bead. (*Lower*) GFP-tagged M6DH on a bead. (*C*) Poisson statistics for actin filament-binding probability. (*Solid line*) The probability, $1 - \exp(-\lambda_m x)$, that a bead carries one or more active M6WT molecules, fit by a least-squares method ($\lambda_m = 0.082$, reduced $\chi^2 = 0.03$). Data are shown as mean $\pm\, n^{1/2}N^{-1}$, where n is the number of beads that moved and N (>79) is the number of trials. (*Dashed line*) The probability that a bead carries two or more active M6WT molecules (reduced $\chi^2 = 0.98$).

filament. Both distributions fit well by a single-exponential curve (M6WT, $\tau = 0.085$ s; M6DH, $\tau = 0.42$ s). ATP turnover time, ~0.11 s, is almost the same as the duration time of attachment for M6WT (29), which also supports that the movement of M6WT without cargo is not processive.

Evidence for cargo transport by a single monomeric myosin-VI molecule

Although M6WT without cargo did not show processive movement, myosin-VI functions as a cargo transporter in cells, suggesting that myosin-VI in cells moves cargos processively. We hypothesized that the cargo binding to myosin-VI may allow the myosin-VI motor to move processively. Because myosin-VI transports 100- to 200-nm-diameter vesicles attached at its tail globular domain in cells (19), we attached a 200-nm-diameter polystyrene bead to this region and observed the bead movement by using an optical trapping nanometry system which enabled us to detect clearly the small and fast movement with nanometer accuracy and high temporal (submillisecond) resolution at low load (24,25). (Fig. 2 *A* and Materials and Methods).

We examined whether the observed bead movement was indeed due to single monomeric myosin-VI molecules. We first determined the fraction of fluorescent GFP tagged to myosin-VI heads by monitoring the photobleach reaction of the fluorescence of the GFP-tagged M6DH attached to a glass surface (30), since it is known that GFP molecules are not always fluorescently active. Based upon the ratio of single-step and double-step photobleach events, the fraction of fluorescently active GFP was determined to be 83% in our assay system. The experimental data described below was corrected based upon this result.

Because myosin-VI was bound to a bead via an antibody for His-tag that has two binding sites for myosin-VI (see Materials and Methods), we first confirmed that myosin-VI bound to the two binding sites of the antibody randomly and not cooperatively through dimerization. GFP-tagged myosin-VI molecules were mixed with antibodies at a molar ratio of 1:10 in solution and incubated for 30 min. This ratio was fivefold higher than that of bead to antibody (1:50) (see Materials and Methods). The fluorescence of complexes spread to a glass surface was observed at the single molecular level (8,27,28). Of the 135 fluorescent spots of GFP observed, the

number of spots showing single-step bleaching was 131 (97.1%) and the number showing double-step bleaching was 4 (2.9%). These fractions are in agreement with the Poisson statistics for random binding of myosin-VI to the antibody.

Second, we confirmed that GFP-tagged M6WT bound to a bead randomly, not cooperatively. When GFP-tagged M6WT molecules were mixed with antibody-coated beads at the stoichiometry of 2:1, 106 out of 152 beads (70%) did not show fluorescence and 46 beads did, indicating that ~30% beads bound fluorescent GFP-tagged M6WT (Fig. 2 *B*). Thirty-seven (24%), 8 (5.2%), and 1 (0.7%) beads out of 152 beads showed single-, double- and triple-step photobleaching, respectively. Considering the fraction of nonfluorescent GFP, the fraction of M6WT bound successfully to the beads is calculated as $(37 \times 1 + 8 \times 2 + 1 \times 3)/0.83/(152 \times 2) = 0.22$. If GFP-tagged M6WT binds randomly to the bead, the number of GFP-tagged M6WT bound to a bead can be given by the Poisson statistics, $P(n) = (\lambda_b N)^n/n!\exp(-\lambda_b N)$, where n is the number of GFP-tagged M6WT molecules bound to a bead, N is the mixing molar ratio of M6WT to bead, and λ_b is the fraction for M6WT to successfully bind to the bead. According to these statistics, when $\lambda_b = 0.22$ and $N = 2$, the fractions of beads showing nonfluorescence, single-step photobleaching, and double-step photobleaching are calculated as $P(0) + P(1) \times (1 - 0.83) = 69\%$, $P(1) \times 0.83 + P(2) \times 2 \times 0.83 \times (1 - 0.83) = 25\%$, and $P(2) \times 0.83^2 + P(3) \times 3 \times 0.83^2 \times (1 - 0.83) = 4.6\%$, respectively. These values are in agreement with the observed values. Thus, the results show that GFP-tagged M6WT bound randomly to antibody-coated beads.

Based on the result that M6WT bound randomly to antibody-coated beads, we used Poisson statistics for actin-filament-binding probability (11,31) to evaluate whether the observed movement of beads was due to single M6WT molecules. The beads coated with antibodies for His-tag were mixed with GFP-tagged M6WT at various ratios of M6WT molecule to bead. The fraction of beads moving continuously (>50 nm) when beads were brought into contact with actin filaments was recorded against various M6WT molecule/bead ratios (Fig. 2 *C*). The data were fit well to the probability function, $1\text{-}\exp(-\lambda_m x)$, describing a bead carrying one or more active M6WT molecules, where x is the M6WT molecule/bead ratio in the mixture solution and λ_m is the fraction of myosin that bound to and moved the bead, 0.082 (Fig. 2 *C*). This result indicates that single monomeric molecules of M6WT are sufficient to move a bead processively. In this study, we observed the movement of M6WT at low M6WT/bead stoichiometries of 1:1 or 2:1. At the M6WT: bead ratio of 2:1, ~6% of beads bound two M6WT molecules. However the percentage of beads that are moved by two monomeric M6WT molecules is calculated as $6\% \times$ (the fraction of active M6WT on the bead, $\lambda_m/\lambda_b = 37\%) \times q$ (<0.5) $< 1.1\%$, where q is the probability that two M6WT molecules (each 50 nm in length) will randomly bind to one bead (200 nm in diameter) and simultaneously interact with an actin filament, and is estimated to be <0.5 (refer to Svoboda and Block (31)). The fraction of beads binding more than two M6WT molecules is negligibly small. Furthermore, the fraction of beads containing two M6WT bound to one antibody molecule when mixed at the stoichiometry of myosin/bead = 2:1 is calculated as (the fraction of beads with M6WT bound, 30%) $\times$ (the probability for two M6WT binding to one antibody, $<2.9\%$) $< 0.87\%$. Thus, these probabilities are too small to explain the fraction of beads moving, 15% (Fig. 2 *C*).

Single wild-type myosin-VI with cargo moves processively

Fig. 3 *A* shows a typical trace of the time course for the stepping movement of M6WT tagged with a bead at no

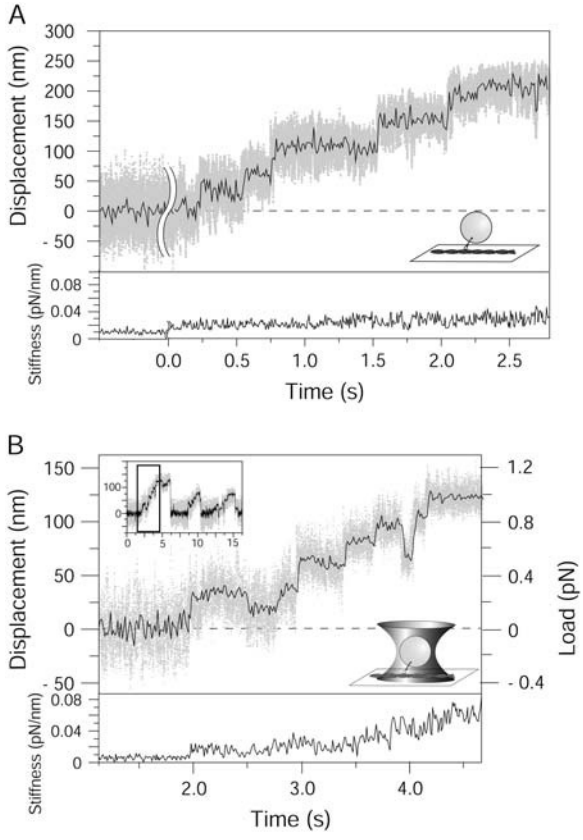

FIGURE 3 Processive steps of cargo-carrying myosin-VI. Stepwise movements of single-headed M6WT with a bead at no load, when the optical trap was off (*A*), and at load, when the trap was on (*B*). In both panels, the upper trace shows displacement and the lower shows stiffness. In panel *A*, interaction occurred just before 0 s, after which the optical trap was turned off. In panel *B*, the interaction started at 2 s, after which stiffness increased. (*Inset*) Trace where trapped bead was stalled and pulled back to the trap center. (*B*) An expanded view of the boxed area in the inset. ATP concentration, 100 μM. (*Gray dots*) raw data; (*black line*) same data passed though a low-pass filter of 20-Hz bandwidth.

external load. The mean step size was 40 nm. M6WT showed steps mostly in one direction, which we define as the forward direction (Fig. 4 *A*, *top panel*, *black bars*). M6WT moved processively even when the optical tweezers was switched on and force was exerted on the beads (Fig. 3 *B*). The mean step size decreased from 40 to 20 nm at maximum load and was independent of ATP concentration ranging from 25 μM to 4 mM (Fig. 4 *B*). The number of backward steps increased with load and was equal to that of forward steps at maximum load (Fig. 4 *A*, *panels 2–4*). In contrast, the M6DH produced mostly forward steps (Fig. 4 *A*, *gray bars*) and the step size was almost constant, independent of the load (Fig. 4 *B*), consistent with a previous report (32). Fig. 4 *C* shows histograms of maximum forces for M6WT (*black bars*) and M6DH (*gray bars*). The mean maximum force of single-headed M6WT (1.0 $\pm$ 0.02 pN) was approximately one-half that of M6DH (1.9 $\pm$ 0.04 pN). We think that the force reaches maximum when the frequency of forward steps balances with that of backward steps. M6DH undergoes more stably forward steps at high load than single-headed M6WT because in the case of M6DH, the bead tethered to an actin filament by the forward head remains longer in the vicinity of the actin filament, allowing more time for the detached rear head to reach the forward actin target. Therefore, the M6DH could develop a maximum force twice as large as the single-headed M6WT. Fig. 4 *D* shows a histogram of run lengths of beads moved by single-headed M6WT at zero load. The mean run length (91 nm) was ~2.5-fold shorter than that of M6DH (~220 nm) (7,8). When the optical tweezers was switched on (trap stiffness; ~8 fN/nm), the mean run length was similar to that without load. Since the step size decreased with load, more steps were observed (Fig. 3 *B*). When we applied the load, the bead was trapped by optical tweezers and so the thermal motions of the bead were suppressed. Therefore, the myosin tagged with the bead could run a longer distance along an actin filament without diffusing away when the load was applied by the optical tweezers.

To investigate the coupling between the ATP turnover and step, we analyzed dwell times of steps at low loads (<0.5 pN) (Supplementary Material, Fig. S1). Stepping rate, defined as the inverse of dwell time, became smaller as ATP concentration decreased. Stepping rate versus ATP concentration fit well to Michaelis-Menten kinetics. The measured maximum stepping rate and Michaelis constant were 8.8 s^{-1} and 250 μM, respectively, consistent with the value from biochemical measurements (29,33), suggesting that each step corresponds to a single cycle of the ATP hydrolysis.

Movement of cargo bound myosin-VI in a high viscous solution

It is thought that myosin-VI transports vesicles in cells for micron-order distance (21). The present results support the idea that the rate of diffusion of myosin-VI from actin

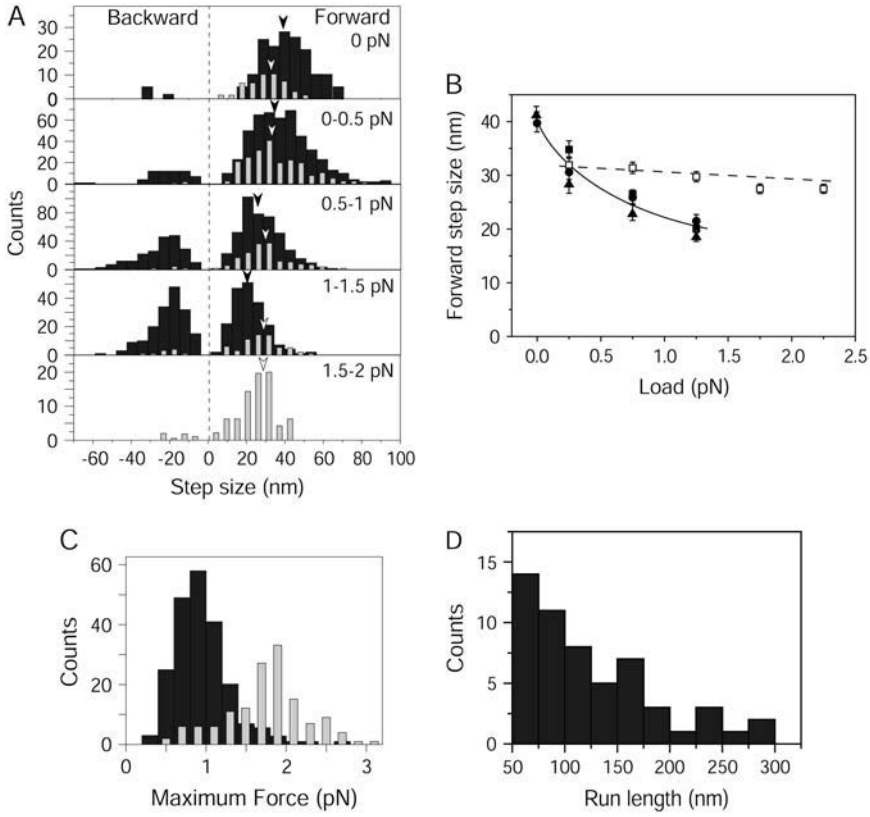

FIGURE 4 Mechanical property of M6WT and M6DH. (*A*) Histograms of step sizes at various loads. (*Black bars*) Single-headed M6WT; (*gray bars*) M6DH. Solid and open arrowheads show mean step size for single-headed M6WT and M6DH, respectively, at various loads as stated in upper right corners. (*B*) Mean step sizes at various loads. Symbols indicate data points (mean $\pm$ SE) for M6WT in the presence of 4 mM ATP (■), 100 μM ATP (●), and 25 μM ATP (▲), and for M6DH in the presence of 4 mM ATP (□). (*Solid line*) Fitting line for mean step-size plots of M6WT. (*Dashed line*) Fitting line for mean step-size plots of M6DH. (*C*) Histograms of maximum force caused by M6WT (*black bars*) and M6DH (*gray bars*). (*D*) A histogram of run length at zero load. ATP concentration is 25–100 μM.

filaments influences the processive movement of myosin-VI. This raises a notion that the run length of myosin-VI may be increased in viscous solution environment in cells in which the viscosity is ~50 times larger than that of water (34). A dense actin meshwork structure is one of the major factors of a high viscosity in cells (35).

To examine the cargo transport by myosin-VI in such a viscous meshwork structure, we examined the movement of bead-bound myosin-VI in a high viscous solution containing methylcellulose (see Materials and Methods for detail), a high-polymer chain composed of trimethyl glucose forming a network structure (36).

At 0.5% (w/v) methylcellulose in the motility buffer, the 200-nm bead underwent slow Brownian motion (40 times slower than that in water) (see Materials and Methods). Fig. 5 *A* shows typical movement of a bead with GFP-tagged M6WT along an actin filament. Green spots indicate fluorescence of GFP-tagged M6WT on the bead (*white arrow*). Fig. 5, *B* and *C*, shows time courses of bead movements along actin filaments (*x* direction) and deviations of the beads in the perpendicular (*y*) direction, respectively. Myosin-VI on beads underwent dissociation and association with the actin filaments and occasionally backward movement, but on average they moved in one direction. We did not observe such long travel distances in the absence of methylcellulose (Fig. 4 *D*). However, the mean travel distance was still hundreds of nanometers. The mean velocity was decreased to be ~100 nm/s compared to that without methylcellulose (40 nm × 8.8 s^{-1} = 352 nm/s).

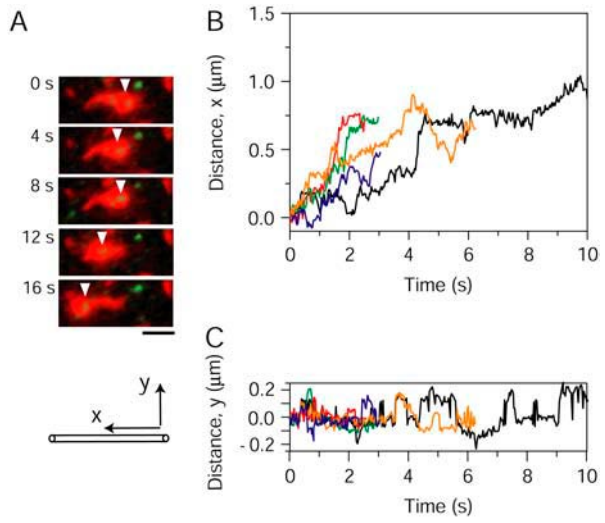

FIGURE 5 Movement of a GFP-tagged M6WT with a bead bound in 0.5% methylcellulose solution. (*A*) Time course of the movement. The bead and an actin filament were labeled with red fluorescent dyes and M6WT was labeled with GFP. Both fluorescences were simultaneously observed by total internal reflection microscopy (27) equipped with double-view optics (52). In the figure, they were artificially colored red and green, respectively. The arrowhead indicates the center of the bead. Frame interval, 4 s; scale bar, 1 μm. (*B*) Typical time courses of the movement of beads by M6WT along actin filaments (*x* direction). Each colored trace indicates the movement of one bead by M6WT. (*C*) Time courses of the movement of beads in *B* perpendicular to the actin filaments (*y* direction). Colors indicate corresponding traces in panels *B* and *C*.

DISCUSSION

We showed that a single-headed M6WT with a bead bound moved processively along an actin filament with large steps. A critical issue is whether the observed processive movement is due to single monomeric M6WT molecules but not multiple or dimerized molecules bound to the bead (because the predicted coiled-coil element exists in the tail domain of M6WT). The results showed that 1), M6WTs were single-headed in electron micrographs; 2), fluorescence from GFP-tagged M6WT bound to a glass surface photobleached in a single step; 3), GFP-tagged M6WT bound to antibody randomly; 4), GFP-tagged M6WT randomly bound to antibody-coated beads; 5), the fraction of beads on which two GFP-tagged M6WT bound to the two binding sites of an antibody was negligibly small; and 6), the Poisson statistics for actin filament-binding probability fit to the probability function, $1 - \exp(-\lambda_m x)$ (see Results). These results provide sufficient evidence that the observed processive movement is indeed due to a single one-headed M6WT molecule with a bead bound. Furthermore, the mechanical properties of M6WT were different from those of myosin-VI engineered to form a dimer (M6DH): 1), the step size depended on the load, whereas that of M6DH was almost independent; 2), the fraction of backward steps at higher load is larger; and 3), the maximum force was approximately one-half that of M6DH.

The results show that a single one-headed M6WT moves processively along an actin filament with large steps upon binding a bead. How does such processive movement occur? The conventional model for an actomyosin motor postulates that the neck domain (calmodulin binding domain) (Fig. 1 *A*) of the myosin head acts as a lever arm, and movement is caused by swinging this lever arm (6,37,38). Myosin-VI, however, has no rigid lever arm long enough to move the bead 40 nm in one step (39,40). Thus, neither the hand-over-hand mechanism nor the conventional lever arm swinging mechanism applies to the single-headed myosin-VI.

The myosin head is attached at its tail end to the bead via a flexible α-helix, ~30 nm long as estimated from the electron micrograph (Fig. 1 *A*). Because the myosin head is much smaller than the bead, it undergoes rapid Brownian motion relative to the bead. If we assume a myosin head diffuses 40 nm at zero load, the time to diffuse this distance is estimated to be 14 μs (see note in Supplementary Material). The bead diffuses ~5 nm in this time (14 μs). The time it takes for a myosin head to diffuse 20 nm at maximum load (1.25 pN) is estimated to be 3.5 μs. The bead diffuses ~2.7 nm in this time even when it is pulled backward by a force of 1.25 pN (see Supplementary Material). The myosin head may not release Pi soon after the myosin head reaches the forward actin target and may be in a weak binding state for a while

(29). However, the myosin head should undergo rapid association and dissociation with actin in the micriosecond time range in the weak binding state (41), so the myosin head tethered to the large bead would stay at the forward actin target until the Pi release. Therefore, the myosin head tethered to the bead via a long (~30-nm) flexible α-helix could detach from actin and reattach to the next target zone without diffusing away from the actin.

Along with being a clathrin-coated vesicle transporter, myosin-VI is also thought to function as an anchor to stabilize membrane tension (42,43). These functions are determined by a tension sensor mechanism caused by strain-dependent regulation of the ATP and ADP binding rates to the myosin head (32). These rates are thought to determine rate-limiting for attachment to and detachment from actin (29).

Based on these facts, we propose processivity is caused by slower Brownian motion of the cargo and preferential landing of the myosin head to the actin filament (Fig. 6). The bead tethered to an actin filament via myosin-VI undergoes Brownian motion. When the bead diffuses toward the minus end of the actin filament (forward direction) a sufficient distance and the myosin head is pulled in the forward direction or the backward strain exerted on the head is relaxed, ATP binding is accelerated (Fig. 6 *A*), consistent with a previous report (32). When ATP binds to the head, the head dissociates from actin and undergoes rapid Brownian motion (Fig. 6 *B*). Then, the head preferentially lands to the next actin target in the forward direction (Fig. 6 *C*), and strongly binds to the actin, accompanied by isomerization of the myosin head (-ADP-Pi) or Pi release (Fig. 6 *D*), shifting the bead 40 nm. The strain dependence of product release of myosin-VI is directionaly reversed compared to that of mysin-V (30), which means that the myosin-VI moves in the opposite direction.

We have previously proposed a strain-sensor model (30,44) to describe the mechanism of preferential landing on the actin target by the myosin head. In this model, a portion of the myosin head, e.g., the neck domain or converter domain (40,45), acts as a strain sensor. This model assumes that when the backward strain is exerted on the head undergoing association and dissociation in the weakly binding state, the isomerization of the myosin or Pi release is accelerated, resulting in strong binding to actin. According to this model, if the dissociated head diffuses to the forward actin target and binds there, a backward strain should be exerted on the head and the head should associate tightly with actin, accompanied by isomerization of the myosin head or Pi release (Fig. 6, *C* and *D*). The isomerization or Pi release may be accompanied by conformational changes (power stroke) in the head (6,37,38) and/or hopping of the head along actin momomers (46,47) to force the cargo forward (Fig. 6 *D*). This conformational change would promote forward preferential landing in the next stepping cycle (12,48). The compatibility between the directions of binding sites of myosin and actin may also be important for the preferential landing to the forward actin target (46).

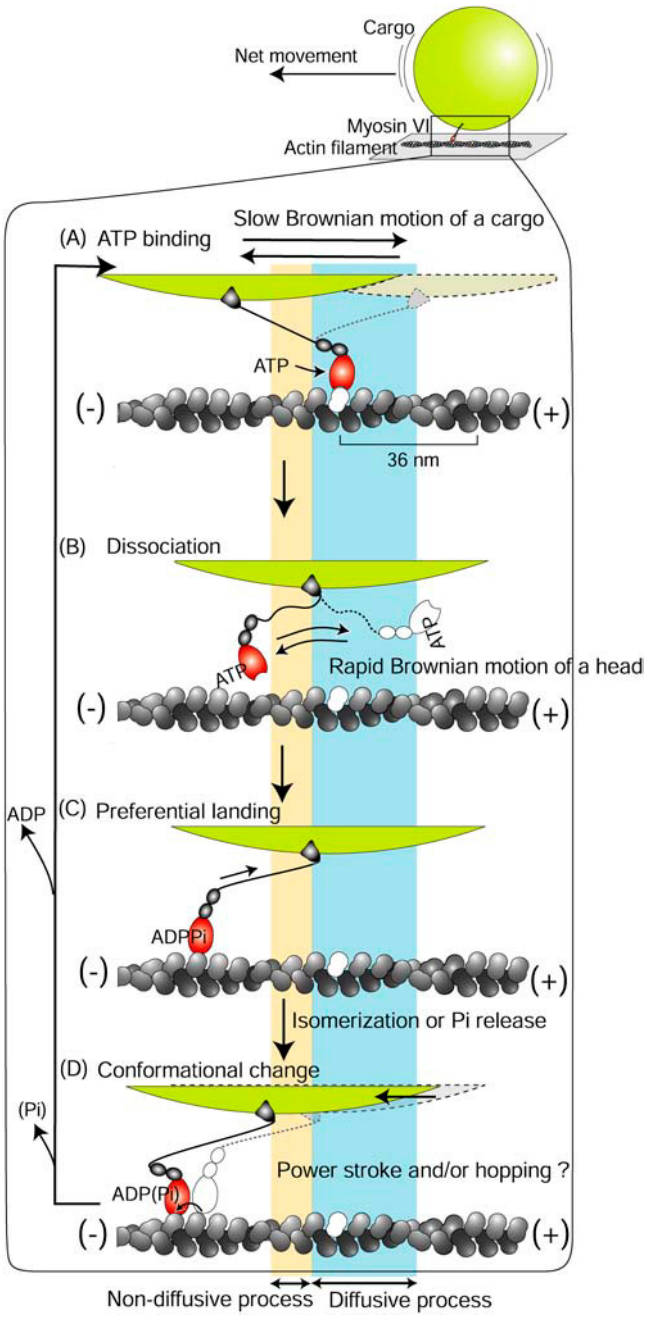

FIGURE 6 A possible mechanism for the processive movement of single-headed cargo carrying myosin-VI. (*A*) A cargo diffuses thermally against the load toward the (−) end of an actin filament (forward direction). Next, ATP binds to the head and dissociates it from actin. (*B*) The dissociated head undergoes rapid Brownian motion over the actin filament. (*C*) The head preferentially lands on the forward actin target before the bead can diffuse away. (*D*) The isomerization of the head or Pi release changes the conformation from a weak to strong bound state. The cargo is moved by 12 nm by power stroke and/or the hopping of the head in this process (see text for details).

To examine whether our mechanism is consistent with the actual mechanical features of myosin-VI, we analyzed the dwell times at various loads (Fig. 7) according to Kramer's first-passage time (48–50). Taking into account that the force-generating step is fast and that ADP release is the rate-liming step at saturating ATP concentration (29), the mean dwell time is approximately given by

$$\tau = \tau_{\mathrm{ADP}} + \tau_{\mathrm{diff}} \exp(Fd/k_{\mathrm{B}}T), \quad (1)$$

where τ_{ADP} is the time for ADP release, d is the displacement caused by the rectified Brownian motion of the bead except for that by the power stroke and/or hopping of the myosin head, τ_{diff} is the time it takes for the bead to diffuse the distance d at zero load, F is the load exerted on the bead, k_{B} is the Boltzmann constant, and T is the absolute temperature. The displacement caused by the power stroke and/or hopping of the head is determined to be 12–18 nm (18,48). If the displacement is 12 nm, d (observed step size – 12 nm) varies from 28 to 8 nm when the load increases from 0 to 1.25 pN (Fig. 4 *B*). τ_{diff} is given by $d^2/2D$, where D is the diffusion constant of the bead, 8.3×10^2 nm^2 ms^{-1} (see Supplementary Material). Thus, the value of $\tau_{\mathrm{diff}} \exp(Fd/kT)$ varies from 0.5 to 0.4 ms with changes in the load from 0 to 1.25 pN. These values are >200 times smaller than τ_{ADP} (110 ms). Even if it is taken into account that the bead may undergo three-dimensional Brownian motion, the contribution of bead diffusion to the dwell time would be negligibly small. Therefore, the dwell time would be almost constant ($\sim\tau_{\mathrm{ADP}}$), independent of the load. This result is consistent with the experimental data (Fig. 7).

Our model is consistent with the 1957 Huxley model (51), in which random diffusive motion of the myosin head is rectified in one direction by an asymmetric binding affinity of the head for actin. Rock et al. (48) also explained the processive movement of M6DH based on the 1957 Huxley model (see Supplementary Material, Fig. S2). We tried to explain our data by their model in which the proximal tail acts as a spring with the constant of ~0.25 pN/nm and the power stroke size is 12 nm. Based on the model of Rock et al., the time required for the proximal tail (spring) to diffuse forward to the next actin binding site when the bead was pulled back by the maximum force, 1.25 pN (Fig. 4 *C*), was calculated to be ~30 μs (assuming one-dimensional Brownian motion of the head and a 13-nm stretch of the proximal tail). The bead would diffuse 11 nm toward the backward direction in this time and the myosin head could not reach the forward actin target zone. Thus, it takes a long time to stretch the proximal tail (spring) for a sufficient distance, so we adopted an additional movement of the cargo in our model (Fig. 6).

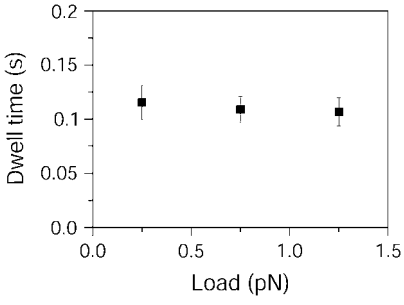

FIGURE 7 Dwell times of steps at various loads. Solid squares indicate data points (mean ± SE) in the presence of 4 mM ATP (n = 57–132). (See text for details.)

In cells, myosin-VI transports endocytic vesicles in a dense actin meshwork structure. This meshwork structure causes high viscosity, ~50 times higher than in water (34). Can our model be applied to the movement of myosin-VI with a cargo bound at such a high viscous environment? The high viscosity caused by a dense actin meshwork structure could affect the diffusion of the cargo but do little to the myosin head because the head is smaller than that of the meshwork structure (35). In such a high viscous condition, the cargo bound myosin-VI frequently detached from actin. But unlike in low viscosity, myosin reattached to the same actin filament due to the diffusion-limited slow Brownian motion of the cargo. This resulted in longer travel distances and slower transport velocity (~100 nm/s) caused by a detached phase. This slower velocity is comparable to that observed in cells (21). The viscous drag force would impose load on the bead, but the load should be negligible ($F = -\gamma v \sim 10$ fN, where γ is a drag coefficient and v is velocity) at the observed velocity (~100 nm/s). The results indicate that our model works successfully at high viscous environments in cells.

The results reported here indicate that single monomeric myosin-VI could transport large cargos such as intracellular vesicles in viscous environment in cells. However, it is likely that multiple molecules are present in single vesicles and this would further facilitate the processive transportation of the cargos (Supplementary Fig. S3). Alternatively, a certain population of myosin-VI assembles to form a dimer in cells, thus facilitating the processive movement of myosin-VI/cargo complex. However, it should be emphasized that the processive nature of myosin-VI/cargo complex observed in this study is the base to explain the physiological function of myosin-VI as a cargo transporter.

SUPPLEMENTARY MATERIAL

An online supplement to this article can be found by visiting BJ Online at http://www.biophysj.org.

We thank Peter Karagiannis for reading the manuscript, Y. Arai for technical advice, and our colleagues for advice and discussion.

REFERENCES

1. Goodson, H. V., and J. A. Spudich. 1993. Molecular evolution of the myosin family: relationships derived from comparisons of amino acid sequences. *Proc. Natl. Acad. Sci. USA.* 90:659–663.

2. Cheney, R. E., M. A. Riley, and M. S. Mooseker. 1993. Phylogenetic analysis of the myosin superfamily. *Cell Motil. Cytoskeleton*. 24:215–223.
3. Hodge, T., and M. J. Cope. 2000. A myosin family tree. *J. Cell Sci.* 113:3353–3354.
4. Cheney, R. E., and M. S. Mooseker. 1992. Unconventional myosins. *Curr. Opin. Cell Biol.* 4:27–35.
5. Mehta, A. D., R. S. Rock, M. Rief, J. A. Spudich, M. S. Mooseker, and R. E. Cheney. 1999. Myosin-V is a processive actin-based motor. *Nature*. 400:590–593.
6. Sakamoto, T., F. Wang, S. Schmitz, Y. Xu, Q. Xu, J. E. Molloy, C. Veigel, and J. R. Sellers. 2003. Neck length and processivity of myosin V. *J. Biol. Chem.* 278:29201–29207.
7. Rock, R. S., S. E. Rice, A. L. Wells, T. J. Purcell, J. A. Spudich, and H. L. Sweeney. 2001. Myosin VI is a processive motor with a large step size. *Proc. Natl. Acad. Sci. USA*. 98:13655–13659.
8. Nishikawa, S., K. Homma, Y. Komori, M. Iwaki, T. Wazawa, A. Hikikoshi Iwane, J. Saito, R. Ikebe, E. Katayama, T. Yanagida, and M. Ikebe. 2002. Class VI myosin moves processively along actin filaments backward with large steps. *Biochem. Biophys. Res. Commun.* 290:311–317.
9. Inoue, A., J. Saito, R. Ikebe, and M. Ikebe. 2002. Myosin IXb is a single-headed minus-end-directed processive motor. *Nat. Cell Biol.* 4:302–306.
10. Walker, M. L., S. A. Burgess, J. R. Sellers, F. Wang, J. A. Hammer 3rd, J. Trinick, and P. J. Knight. 2000. Two-headed binding of a processive myosin to F-actin. *Nature*. 405:804–807.
11. Rief, M., R. S. Rock, A. D. Mehta, M. S. Mooseker, R. E. Cheney, and J. A. Spudich. 2000. Myosin-V stepping kinetics: a molecular model for processivity. *Proc. Natl. Acad. Sci. USA*. 97:9482–9486.
12. Veigel, C., F. Wang, M. L. Bartoo, J. R. Sellers, and J. E. Molloy. 2002. The gated gait of the processive molecular motor, myosin V. *Nat. Cell Biol.* 4:59–65.
13. Forkey, J. N., M. E. Quinlan, M. A. Shaw, J. E. Corrie, and Y. E. Goldman. 2003. Three-dimensional structural dynamics of myosin V by single-molecule fluorescence polarization. *Nature*. 422:399–404.
14. Yildiz, A., J. N. Forkey, S. A. McKinney, T. Ha, Y. E. Goldman, and P. R. Selvin. 2003. Myosin V walks hand-over-hand: single fluorophore imaging with 1.5-nm localization. *Science*. 300:2061–2065.
15. Wells, A. L., A. W. Lin, L. Q. Chen, D. Safer, S. M. Cain, T. Hasson, B. O. Carragher, R. A. Milligan, and H. L. Sweeney. 1999. Myosin VI is an actin-based motor that moves backwards. *Nature*. 401:505–508.
16. Yildiz, A., H. Park, D. Safer, Z. Yang, L. Q. Chen, P. R. Selvin, and H. L. Sweeney. 2004. Myosin VI steps via a hand-over-hand mechanism with its lever arm undergoing fluctuations when attached to actin. *J. Biol. Chem.* 279:37223–37226.
17. Okten, Z., L. S. Churchman, R. S. Rock, and J. A. Spudich. 2004. Myosin VI walks hand-over-hand along actin. *Nat. Struct. Mol. Biol.* 11:884–887.
18. Lister, I., S. Schmitz, M. Walker, J. Trinick, F. Buss, C. Veigel, and J. Kendrick-Jones. 2004. A monomeric myosin VI with a large working stroke. *EMBO J.* 23:1729–1738.
19. Buss, F., S. D. Arden, M. Lindsay, J. P. Luzio, and J. Kendrick-Jones. 2001. Myosin VI isoform localized to clathrin-coated vesicles with a role in clathrin-mediated endocytosis. *EMBO J.* 20:3676–3684.
20. Frank, D. J., T. Noguchi, and K. G. Miller. 2004. Myosin VI: a structural role in actin organization important for protein and organelle localization and trafficking. *Curr. Opin. Cell Biol.* 16:189–194.
21. Aschenbrenner, L., S. N. Naccache, and T. Hasson. 2004. Uncoated endocytic vesicles require the unconventional myosin, Myo6, for rapid transport through actin barriers. *Mol. Biol. Cell*. 15:2253–2263.
22. Harada, Y., A. Noguchi, A. Kishino, and T. Yanagida. 1987. Sliding movement of single actin filaments on one-headed myosin filaments. *Nature*. 326:805–808.
23. Ishijima, A., H. Kojima, T. Funatsu, M. Tokunaga, H. Higuchi, H. Tanaka, and T. Yanagida. 1998. Simultaneous observation of individual ATPase and mechanical events by a single myosin molecule during interaction with actin. *Cell*. 92:161–171.
24. Nishiyama, M., E. Muto, Y. Inoue, T. Yanagida, and H. Higuchi. 2001. Substeps within the 8-nm step of the ATPase cycle of single kinesin molecules. *Nat. Cell Biol.* 3:425–428.
25. Okada, Y., H. Higuchi, and N. Hirokawa. 2003. Processivity of the single-headed kinesin KIF1A through biased binding to tubulin. *Nature*. 424:574–577.
26. Kojima, H., E. Muto, H. Higuchi, and T. Yanagida. 1997. Mechanics of single kinesin molecules measured by optical trapping nanometry. *Biophys. J.* 73:2012–2022.
27. Funatsu, T., Y. Harada, M. Tokunaga, K. Saito, and T. Yanagida. 1995. Imaging of single fluorescent molecules and individual ATP turnovers by single myosin molecules in aqueous solution. *Nature*. 374:555–559.
28. Iwane, A. H., T. Funatsu, Y. Harada, M. Tokunaga, O. Ohara, S. Morimoto, and T. Yanagida. 1997. Single molecular assay of individual ATP turnover by a myosin-GFP fusion protein expressed in vitro. *FEBS Lett.* 407:235–238.
29. De La Cruz, E. M., E. M. Ostap, and H. L. Sweeney. 2001. Kinetic mechanism and regulation of myosin VI. *J. Biol. Chem.* 276:32373–32381.
30. Watanabe, T. M., H. Tanaka, A. H. Iwane, S. Maki-Yonekura, K. Homma, A. Inoue, R. Ikebe, T. Yanagida, and M. Ikebe. 2004. A one-headed class V myosin molecule develops multiple large (approximately 32-nm) steps successively. *Proc. Natl. Acad. Sci. USA*. 101: 9630–9635.
31. Svoboda, K., and S. M. Block. 1994. Force and velocity measured for single kinesin molecules. *Cell*. 77:773–784.
32. Altman, D., H. L. Sweeney, and J. A. Spudich. 2004. The mechanism of myosin VI translocation and its load-induced anchoring. *Cell*. 116:737–749.
33. Robblee, J. P., A. O. Olivares, and E. M. De La Cruz. 2004. Mechanism of nucleotide binding to actomyosin VI: Evidence for allosteric head-head communication. *J. Biol. Chem.* 279:38608–38617.
34. Boal, D. H. 2002. Mechanics of the Cell. Cambridge University Press, Cambridge, UK.
35. Potma, E. O., W. P. de Boeij, L. Bosgraaf, J. Roelofs, P. J. van Haastert, and D. A. Wiersma. 2001. Reduced protein diffusion rate by cytoskeleton in vegetative and polarized dictyostelium cells. *Biophys. J.* 81:2010–2019.
36. Nishinari, K., K. E. Hofmann, K. Kohyama, H. Moritaka, N. Nishinari, and M. Watase. 1993. Polysaccharide-protein interaction: a rheological study of the gel-sol transition of a gelatin-methylcellulose-water system. *Biorheology*. 30:243–252.
37. Spudich, J. A. 2001. The myosin swinging cross-bridge model. *Nat. Rev. Mol. Cell Biol.* 2:387–392.
38. Moore, J. R., E. B. Krementsova, K. M. Trybus, and D. M. Warshaw. 2004. Does the myosin V neck region act as a lever? *J. Muscle Res. Cell Motil.* 25:29–35.
39. Bahloul, A., G. Chevreux, A. L. Wells, D. Martin, J. Nolt, Z. Yang, L. Q. Chen, N. Potier, A. Van Dorsselaer, S. Rosenfeld, A. Houdusse, and H. L. Sweeney. 2004. The unique insert in myosin VI is a structural calcium-calmodulin binding site. *Proc. Natl. Acad. Sci. USA*. 101:4787–4792.
40. Menetrey, J., A. Bahloul, A. L. Wells, C. M. Yengo, C. A. Morris, H. L. Sweeney, and A. Houdusse. 2005. The structure of the myosin VI motor reveals the mechanism of directionality reversal. *Nature*. 435:779–785.
41. Brenner, B. 1991. Rapid dissociation and reassociation of actomyosin cross-bridges during force generation: a newly observed facet of cross-bridge action in muscle. *Proc. Natl. Acad. Sci. USA*. 88:10490–10494.
42. Hasson, T. 2003. Myosin VI: two distinct roles in endocytosis. *J. Cell Sci.* 116:3453–3461.
43. Warner, C. L., A. Stewart, J. P. Luzio, K. P. Steel, R. T. Libby, J. Kendrick-Jones, and F. Buss. 2003. Loss of myosin VI reduces secretion and the size of the Golgi in fibroblasts from Snell's waltzer mice. *EMBO J.* 22:569–579.

44. Yanagida, T., S. Esaki, A. H. Iwane, Y. Inoue, A. Ishijima, K. Kitamura, H. Tanaka, and M. Tokunaga. 2000. Single-motor mechanics and models of the myosin motor. *Philos. Trans. R. Soc. Lond. B Biol. Sci.* 355:441–447.

45. Houdusse, A., V. N. Kalabokis, D. Himmel, A. G. Szent-Gyorgyi, and C. Cohen. 1999. Atomic structure of scallop myosin subfragment S1 complexed with MgADP: a novel conformation of the myosin head. *Cell.* 97:459–470.

46. Kitamura, K., M. Tokunaga, S. Esaki, A. H. Iwane, and T. Yanagida. 2005. Mechanism of muscle contraction based on stochastic properties of single actomyosin motors observed *in vitro*. *BIOPHYSICS*. 1:1–19. (http://www.jstage.jst.go.jp/browse/biophysics).

47. Okada, T., K. Kitamura, H. Tanaka, A. Hikikoshi Iwane, M. Ikebe, and T. Yanagida. 2005. A single-headed myosin V moves along an actin filament with ~5.6 nm steps. *Joint 61st Harden Conference/EMBO Workshop, Cambridge, UK. Abstract 8.*

48. Rock, R. S., B. Ramamurthy, A. R. Dunn, S. Beccafico, B. R. Rami, C. Morris, B. J. Spink, C. Franzini-Armstrong, J. A. Spudich, and H. L. Sweeney. 2005. A flexible domain is essential for the large step size and processivity of myosin VI. *Mol. Cell.* 17:603–609.

49. Kramers, H. A. 1940. Brownian motion in a field of force and the diffusion model of chemical reactions. *Physica.* 7:284–304.

50. Howard, J. 2001. Mechanics of Motor Proteins and the Cytoskeleton. Sinauer Associates, Sunderland, MA.

51. Huxley, A. F. 1957. Muscle structure and theories of contraction. *Prog. Biophys. Biophys. Chem.* 7:255–318.

52. Kinosita, K., Jr., H. Itoh, S. Ishiwata, K. Hirano, T. Nishizaka, and T. Hayakawa. 1991. Dual-view microscopy with a single camera: real-time imaging of molecular orientations and calcium. *J. Cell Biol.* 115:67–73.